

Article

Exploring the Application of a Debris Flow Likelihood Regression Model in Mediterranean Post-Fire Environments, Using Field Observations-Based Validation

Michalis Diakakis ^{1,*}, Spyridon Mavroulis ¹, Emmanuel Vassilakis ² and Vassiliki Chalvatzi ¹

¹ Department of Dynamic Tectonic and Applied Geology, Faculty of Geology and Geoenvironment, National and Kapodistrian University of Athens, 15784 Panepistimioupoli Zografou, Greece

² Department of Geography and Climatology, Faculty of Geology and Geoenvironment, National and Kapodistrian University of Athens, 15784 Panepistimioupoli Zografou, Greece

* Correspondence: diakakism@geol.uoa.gr; Tel.: +30-210-727-4409

Abstract: Post-fire geomorphic processes and associated risks are an important threat in Mediterranean environments. Currently, post-fire mass movement prediction has limited applications across the Mediterranean despite the abundance of both forest fires and landslide/debris flow disasters. This work applies a debris flow generation likelihood model to evaluate the probability of mass movement phenomena in different catchments of a burnt area, after a catastrophic fire near Schinos (Attica, Greece) in 2021. Then, it uses field observations from the area, recording mass movement phenomena after high-intensity rainfall events, to validate the results. The findings show that the model is successful in determining the probability of debris flow generation in the 21 basins of the study area, ranging from 0.05 to 0.893. The probability values show a statistically significant correlation (sig. = 0.001) with the actual debris flow occurrences in the area, and satisfactory results in terms of the model's predictive ability, functioning well within the particular geo-environmental characteristics of the Mediterranean environment. The results establish the reliability of the approach as a tool to assess mass movement risks in a region with an abundance of post-fire related hazards and disastrous events.

Keywords: debris flow; post-fire; likelihood regression model; Mediterranean environment



Citation: Diakakis, M.; Mavroulis, S.; Vassilakis, E.; Chalvatzi, V. Exploring the Application of a Debris Flow Likelihood Regression Model in Mediterranean Post-Fire Environments, Using Field Observations-Based Validation. *Land* **2023**, *12*, 555. <https://doi.org/10.3390/land12030555>

Academic Editors: Irene Manzella and Bouchra Haddad

Received: 19 January 2023

Revised: 17 February 2023

Accepted: 23 February 2023

Published: 24 February 2023



Copyright: © 2023 by the authors. Licensee MDPI, Basel, Switzerland. This article is an open access article distributed under the terms and conditions of the Creative Commons Attribution (CC BY) license (<https://creativecommons.org/licenses/by/4.0/>).

1. Introduction

Despite the fact that forest fires are an integral part of the Mediterranean ecosystems, their occurrence affects, often heavily, the hydrologic and geomorphic processes, inducing significant changes in the burnt landscape, as well as important subsequent hazards, including erosion [1,2], desertification, soil loss [3,4], and flood and mass movement phenomena [5,6]. One of the most common hazards of a post-fire environment is the occurrence of debris flows of various magnitudes [7–10], triggered by intense rainfall events mobilizing sediments of various grain sizes (from clay to boulders) [11]. Together with water, sediments flow by gravity downstream causing severe impacts, posing a risk to the population [12–16].

Debris flows concentrate large amounts of material due to intensified erosion in post-fire environments, occurring through various mechanisms, including increased weathering of bedrock surfaces [17,18], enhanced slope instabilities [5], and removal of vegetation due to burning (including the root system) [19,20]. In addition, reduced protective ground cover, lack of vegetation canopy [17], changes in soil properties [21], decreased infiltration and increased runoff [1,17,22] can intensify erosion processes. Moreover, other landscape characteristics, beyond the fire, can influence debris flow generation and mass movement, including geological attributes [23], or the presence of fine-grained material [24,25].

Despite their significance and frequency, there is no systematic diagnosis of debris flow risks after forest fires in the Mediterranean region [26]. Current practice in the area bases debris flow prediction on forecasted (or accumulated) rainfall or analysis of historical events [26,27]. In addition, there is extensive literature on rainfall thresholds for triggering landslides and debris flows [28,29]. These approaches have significant value but bear weaknesses in terms of the spatial dimension of occurrence prediction within the fire-hit area, not capitalizing terrain-specific factors that have been associated with debris flow generation. This spatial distinction of debris flow generation risks is particularly useful in planning, prioritizing and placing post-fire protection measures and informing citizens on high-risk locations, allowing for informed decisions when it comes to land use and risk management. Given the catastrophic forest fires of the last decades across the Mediterranean [30] and Greece in particular [31,32], it is important to exploit all the tools available to assess in depth subsequent fire-induced risks. This need becomes even more pressing when we take into account the expected increase in such events due to climate change [33–35], as well as the persistence of debris flow hazards for years after fire containment [5,17,36–38].

In the last few years, witnessing debris flow disasters in different places of the world, the research community, and the community of risk-professionals gradually developed mostly empirical methods for debris flow prediction and warning. These approaches include the use of rainfall thresholds [39–43], the analysis of features of the burnt area [44], and other approaches that are focusing on determining the conditions that may lead to debris flow occurrence [45–47]. Some of the most elaborate of these models and the most commonly used have been developed for the Western U.S. [36,47–50], a part of the world that in many respects (geo-environmental, geomorphological and climatological setting) has similarities with the Mediterranean region. The models developed for the Western U.S. employ mostly binary logistic regression to predict debris flow occurrence based on statistically significant associations of various factors with the outcome of a storm on the landscape [49–51].

In this context, this work examines the applicability of a debris flow likelihood model used in the Western U.S., by introducing its application to the Eastern Mediterranean region, using European soil data to estimate the probability of debris flow occurrence in the post-fire environment of Schinos-Aleporochori in Attica, Greece, after a catastrophic fire in 2021. Then, by monitoring the area and carrying out field observations, this study assesses the model's results by comparing them to actual debris flow occurrences in the fire-hit region.

2. Study Area

2.1. Setting

The study area is located at the northern slope of Geraneia Mt. Administratively, its eastern end belongs to the Attica Region, while its western part to the Corinth Regional Unit of Peloponnese Region. It extends generally from Loutraki in the south to the southern shores of the Alkyonides Gulf in the north and from Megara in the east to Perachora in the west (Figure 1). It is 30 km long in the E-W direction, 13 km wide in the N-S direction and has a perimeter of 125 km. Thus, it forms a natural barrier between central mainland Greece and the Peloponnese, a natural obstacle that should be circumvented, either via its northern or southern sides. The northern pass involves a long and tedious detour, so the most straightforward corridor runs along the southern flank, which has been known under the name of Kakia Skala, i.e., the Skironian Rocks of the antiquity.

Geraneia has all the characteristic properties of mountains close to the sea. Its peak (Makryplagi, 1369 m) is located at a distance of only 4.5 km from the coastline, it is a rocky mountain with considerable relief comprising very deep gorges and steep slopes dropping down both towards the Corinth and the Saronic Gulfs, to the north and south, respectively. This intense morphology is attributed to the geological and neotectonic structure of the mountain. It consists of alpine formations and post-alpine deposits [52–54]. It comprises outcrops of Mesozoic carbonate rocks, tectonically overlain by an ophiolitic

suite, which consists of peridotite, and serpentinite, mafic bodies, shales and cherts. The ophiolites are observed at the central part of the mountain and its northern flanks, while the Mesozoic carbonate outcrops prevail in the eastern, western and southern parts of the Geraneia Mt. The post-alpine deposits are unconformably deposited over the alpine formations and include alluvial deposits and recent scree and talus cones of Holocene age and marine, fluvio-terrestrial and lagoonal deposits of Pliocene and Pleistocene age (Figure S1 in Supplementary Material).

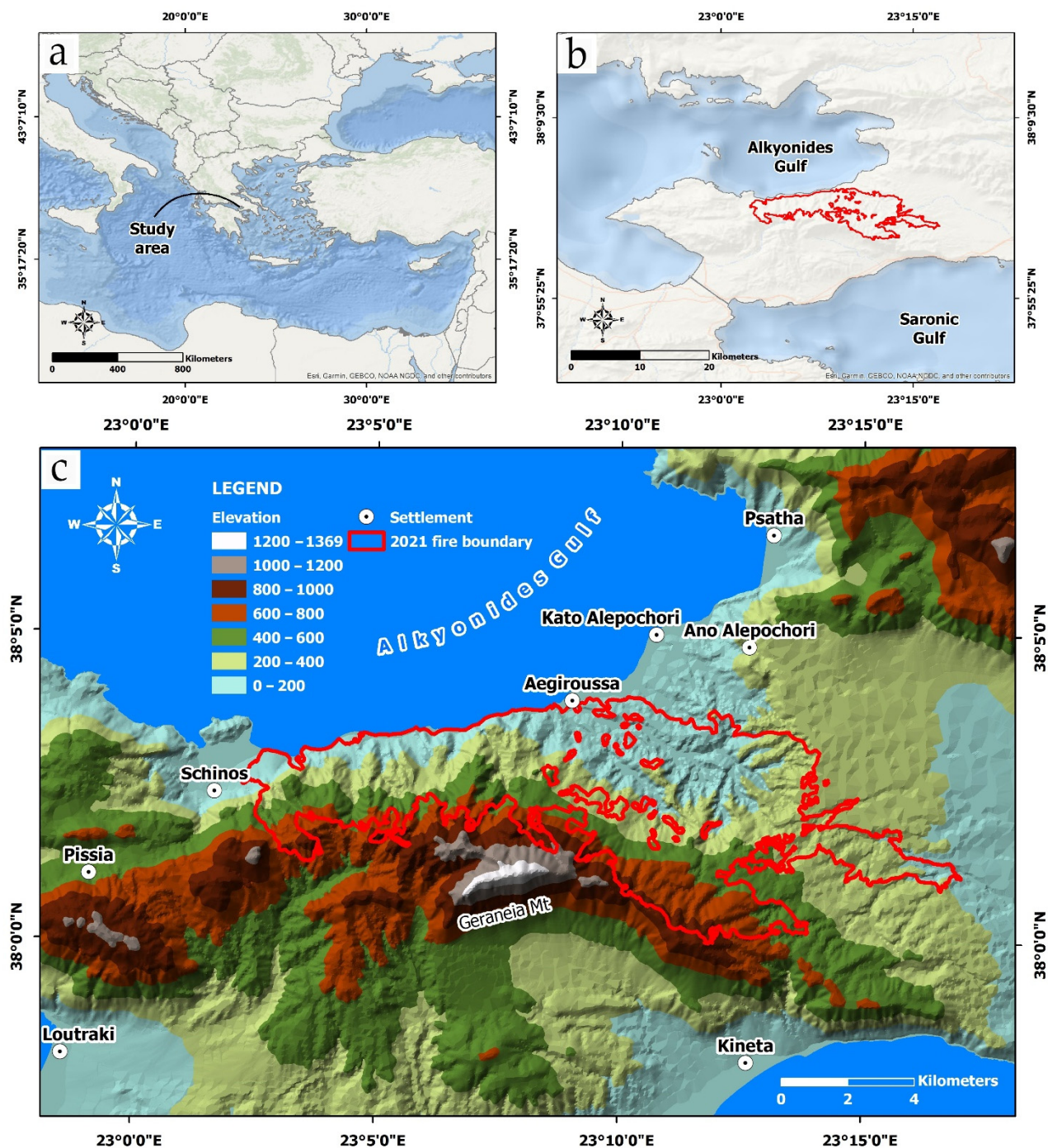


Figure 1. Map of the study area showing (a) its general location in the Eastern Mediterranean, (b) its position between the Alkyonides and the Saronic Gulf in Greece, and the boundary of the May 2021 fire (red-colored line), and (c) the main settlements and elevation in relation to the extent of the 2021 fire.

The studied drainage basins have been formed in the northern slopes of Geraneia and they consist of both alpine formations and post-alpine deposits [52]. The first formations comprises limestone-dolomite of Middle-Upper Triassic–Middle Jurassic and a Middle-Upper Jurassic schist-chert formation, while the latter contain Pliocene and Pleistocene alternations of clays, sands, sandstones and conglomerates, Pleistocene scree and talus cones, alluvial and coastal sand deposits [52].

As regards neotectonics and active tectonics of the area, the area is disrupted by seismic faults, which are responsible for the uplift of Geraneia Mt and the related intense relief. The most important faults in the study area are the oblique-normal, north-throwing onshore Schinos and Pissia faults formed at the western end of the studied basins and the offshore Alepochori fault located north of the basin outlets [55–57] creating sharp relief in the area.

The 1981 earthquake sequence occurred in the eastern part of the Corinth Gulf and included three strong earthquakes with magnitude $M_s = 6.7$, $M_s = 6.4$ and $M_s = 6.3$ generated on 24, 25 February and 4 March 1981, respectively [55,58], resulting in 20 fatalities, 500 injured people and severe non-structural and structural damage to thousands of structures in the earthquake-affected regions of Boeotia, Attica and Corinth [59]. Taking into account all geological and seismological data for the earthquake affected area, it is revealed that all earthquakes were caused by normal faults, which dominate the area and accommodate N-S extension. In addition to the effects on the built environment, these earthquakes caused a large number of primary and secondary effects including extensive primary surface faulting and significant coastal uplift and subsidence in Schinos, Pissia and Alepochori areas, rockfalls, onshore and offshore landslides, liquefaction phenomena and a weak tsunami [60,61].

The synergy of the active tectonics, the intensely fractured and brecciated limestones and the highly tectonized and weathered outcrops of the ophiolites on the northern slopes of the Geraneia, where the studied basins are formed, result in the occurrence of extensive slope movements. These phenomena comprise the frequent generation of rockfalls, which are greatly increased when triggering events such as earthquake and rainfall take place, and debris flows whose probability of occurrence increases especially after the occurrence of forest fires in the area. The latter follow the course of torrents that discharge into the Alkyonides Gulf.

Regarding the hydrology of the study area, 21 drainage basins (shown in Figure 2) have been formed in along the northern slopes of Geraneia Mt, with an approximate N-S direction and area ranging from 0.09 to 34.96 km². All these catchments (in this study named “B1”, “B2”, . . . , “B21”) drain into the southern part of the Alkyonides Gulf (Figure 2).

The drainage network of the wider area is developed over both alpine formations and post-alpine deposits. It is characterized as parallel or even parallel in places, with the streams showing a high length-to-width ratio. The arrangement of the streams is largely asymmetrical, which is mainly attributed to the influence of active tectonics of the area. In general, the drainage system is considered dense. The streams show intense incision upstream, while downstream deposition from mass wasting events prevails and alluvial fans have been formed.

With regard to vegetation according to the classification of forest vegetation as made by Dafis [62] for the vegetation zones in Greece, the study area belongs to the Euromediterranean vegetation zone (*Quercetalia ilicis*). Before the 2021 fire, the area was covered by characteristic forests of *Pinus halepensis* and in several sites by new plantations and dense stands of *Pinus halepensis* and evergreen broadleaves after earlier localized small fires. Apart from *Pinus*, the area hosted *Cypressus sempervirens* and lower vegetation such as *Arbutus Andrachne*, *Cercis Siiquastrum*, *Erica arborea*, *Quercus coccifera*, *Pistacia lentiscus* and other typical of the environment [63].

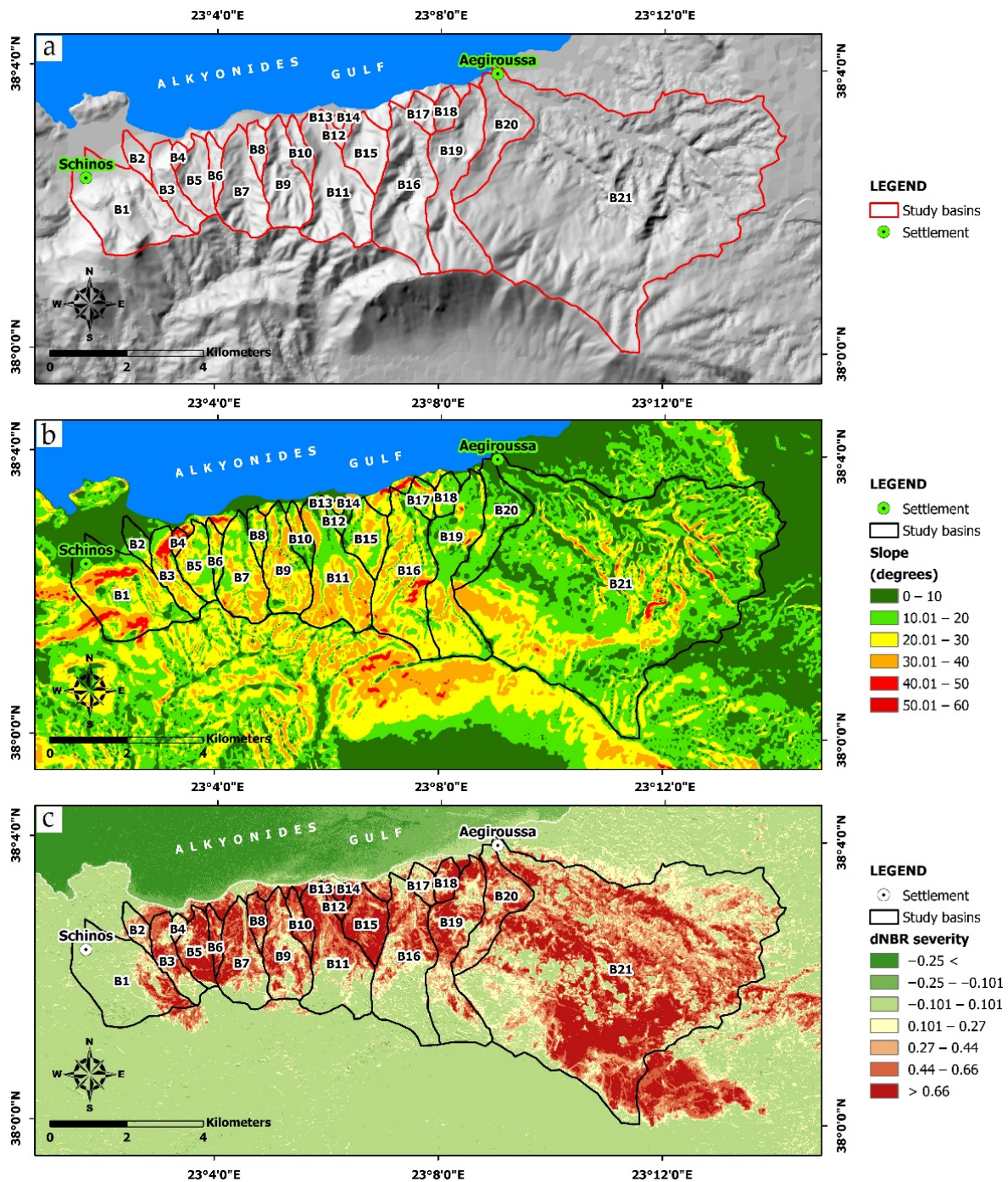


Figure 2. Maps of the study basins against (a) the local relief, (b) the slope inclination of the study area, and (c) the burnt area along with dNBR burn severity.

2.2. The 2021 Fire Event

On 19 May 2021 (21:45 local time), a forest fire broke out in a grassland located east of Schinos area, close to a forest. Open-field burning of agricultural remains has been speculated to be the cause of the forest fire. Due to extreme weather conditions including up to 8 Beaufort wind gusts, fire spread quickly eastwards and affected several villages situated on the northern slopes of Geraneia Mt [64] mainly along the coast. The fire boundary in the north reached the coastal zone (Figure 3), while the burnt slopes with abundant loose material drained directly to the Gulf of Alkyonides (Figure S2 in the Supplementary Material).

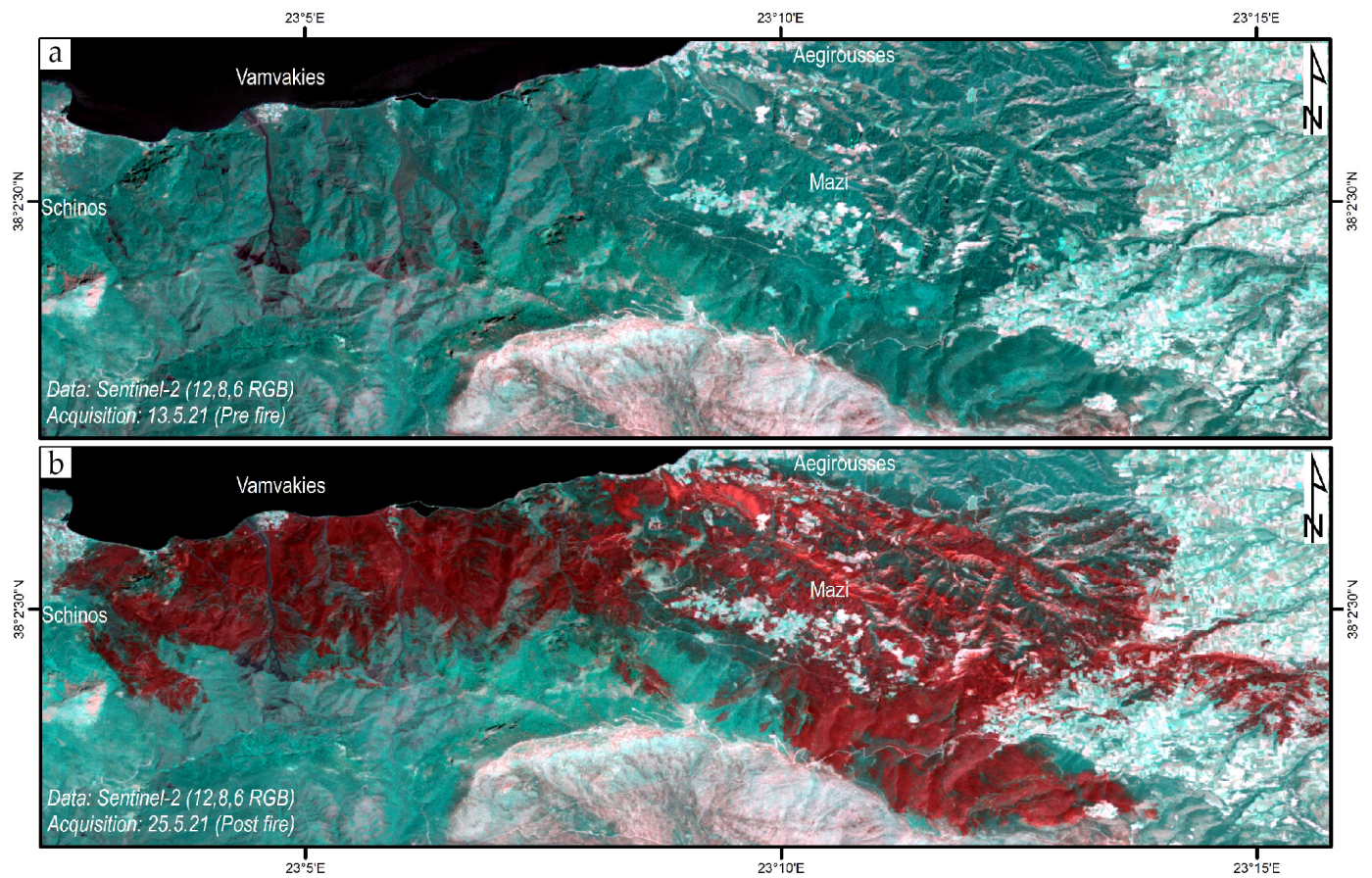


Figure 3. Sentinel-2A satellite images of the study area (a) on 13 May 2021 before the fire and (b) on 25 May 2021 after the fire. The dark red colors show the burnt area.

The synergy of the intense relief of the tectonically active area, the wind gusts of gale force (value 8 in Beaufort wind force scale) and the dense vegetation facilitated the spread of fire and made it difficult to extinguish. On 20 May, the forest fire entered Attica Region. Part of the fire smoke was transported over Attica basin resulting in a gradual increase in particulate matter ($PM_{2.5} > 100 \mu\text{g}/\text{m}^3$) in many districts, as recorded in real time by the Panacea Research Infrastructure network of sensors [65] revealing poor to extremely poor air quality as a result of the fire.

Due to the spread of the fire near residential areas including villages in the coastal area from Schinos to Alepochori and on the northern slopes of Gerania Mt, the 112 Emergency Communications Service was activated three times by sending emergency alert and warning/evacuation messages to residents and visitors of the fire-affected area. The involved Civil Protection authorities evacuated over 10 villages during the evolution of the phenomenon. On 20 May 2021, the Rapid Mapping of the Copernicus Emergency Management Service was activated in order to delineate the boundary of the fire-affected area [66]. The extent of the fire-affected area was 5664.1 ha on 20 May and 6647 ha on 26 May based on products with spatial resolution of 12 m [66]. Based on PlanetScope imagery with approximately 3 m per pixel resolution [67], Lekkas et al. (2021) calculated the total extent of the fire-affected area at 46,687 decares composed of coniferous forest (75.49%), shrublands (15.51%), arable land (8.33%), open shrublands (0.60%) and permanent crops (0.08%) and scattered unaffected patches. Approximately 6414 decares (13.74%) of the fire-affected area were formally protected by the Natura 2000 network. As regards the fire impact on the built environment, houses and infrastructure were affected.

As regards the fire impact on the built environment and structures, the fire affected mainly illegally built houses and a livestock unit with sheep located in Mavrolimni area.

Furthermore, two small boats at the Mavrolimni fishing shelter were burnt along with fish cage materials lying on the beach on the eastern edge of the shelter. Regarding the impact on the livestock, the fire affected beehives and the livestock in the aforementioned unit. The fire history of the area comprises a fire on 3 August 1986, outside the current study area, burning through the forest of the entire southern slope of Geraneia Mt after traveling a distance of about 7 km within almost three hours. In a similar event, the southern slopes of Geraneia Mt (outside the study area) were burned in the 2018 Kineta fire.

3. Materials and Methods

3.1. Approach

One of the most commonly used models for determining the likelihood of a debris flow occurrence is logistic regression, assuming a binary dependent variable denoting the response of catchment to a storm [43,50,51,68,69]. This type of approach, in general, seeks to characterize debris-flow hazard through association of geospatial data describing catchment geomorphology and soil properties, as well as burn severity and storm magnitude, with the occurrence or non-occurrence of a debris flow (binary response). In this context, the statistical likelihood of a debris-flow generation is calculated based on binary logistic regression, using the logistic curve and is given from the following Equation (1) [50]:

$$P = e^x / (1 + e^x) \quad (1)$$

where P represents the statistical likelihood number ranging from 0 to 1, (with higher values denoting higher likelihood of debris flow generation), x is the link function (2), which is given through the following equation (Equation (2)) and e^x is the exponential function (e is the Euler's number and equal to 2.718)

$$x = \beta + (C_1 \times X_1) + (C_2 \times X_2) + \dots + (C_n \times X_n) \quad (2)$$

where β , C_1 , C_2 , \dots , C_n are parameters derived empirically, whereas X_1 , X_2 , \dots , X_n represent independent variables that have an influence on the binary outcome (that is debris flow generation).

The model selected and tested in the present study, is the one developed by Staley et al. [50] that is currently operational in the Western United States [70]. Apart from its proven value, this model was selected because of its relatively low data requirements and the fact that it has been shown to function in a geo-environmental setting similar to that of Greece, characterized by sharp relief and high inclination shaped by active tectonics, similarities in geology, soil and vegetation, as well as semi-arid landscape and climate [71–74].

In the Staley et al. [50] model, the β , C_1 , C_2 , C_3 parameters are determined, as shown in Equation (3).

$$x = -3.63 + (0.41 \times X_1R) + (0.67 \times X_2R) + (0.7 \times X_3R) \quad (3)$$

where

P denotes the statistical likelihood of debris-flow generation;

X_1R denotes the part of upslope area classified as high or moderate soil burn severity and with gradients $\geq 23^\circ$, multiplied by the peak 15 min rainfall accumulation of the design storm (in millimeters [mm]);

X_2R denotes the average differenced normalized burn ratio (dNBR/1000) of the upstream area, multiplied by the peak 15 min rainfall accumulation of the design storm (in millimeters [mm]);

X_3R denotes the soil KF-Factor of the upslope area multiplied by the peak 15 min rainfall accumulation of the design storm (in millimeters [mm]).

3.2. Data Collection

To calculate slope inclination, we used elevation data derived from the Greek land registry service (Hellenic Cadastre), which were part of the national digital elevation raster data of 5 m × 5 m resolution [75]. We obtained slope values using the “Slope” tool of Spatial Analyst toolset of ArcGIS software [76].

The 15 min rainfall maximum accumulation of the design storm for the area was based on local IDF curves published by the Ministry of the Environment and Energy [77]. Given the small size of the area (69 km² in total and just 18.7 km in width) in contrast with the relatively low resolution of IDF estimation, and the fact that the catchments in question have very similar elevation range and morphology, we assumed the same value of rainfall (i.e., the peak 15 min rainfall accumulation of the design storm equal to 15.2 mm) is valid for the whole area.

We used the differential Normalized Burn Ratio (dNBR) index for estimating burn severity. This methodology concerns the generation of raster layers coming from the processing of satellite imagery acquired before and after a fire event, recording the pre- and post-fire conditions. The bands that participate in this raster calculation procedure (we used the Raster Calculator tool of ArcGIS software [76]) cover the Near Infrared and the Short-Wave Infrared wavelength parts of the spectrum. Specifically, we used the 10 m resolution Sentinel-2A B08 and B12 bands, respectively, extracted from two image datasets with a 12-day time difference, before (13.5.21) and after (25.5.21) the event, for the generation of two NBR raster layers. Each 100 square meter pixel obtains a new value after the following calculation shown in the following equation, and this raster processing is repeated twice for both datasets.

$$\text{NBR} = (\text{B08} - \text{B12}) / (\text{B08} + \text{B12}) \quad (4)$$

The next step requires the calculation of dNBR which is achieved after subtracting the post-fire NBR values from the pre-fire NBR values (Equation (5)) for each pixel (Figure 2).

$$\text{dNBR} = \text{NBR}_{\text{pre-fire}} - \text{NBR}_{\text{post-fire}} \quad (5)$$

Finally, we reclassified the resulting raster layer into 5 categories, namely: Unburned, Low Severity, Moderate Severity, High Severity, and Increased Greenness.

Given the lack of field-validated soil burn severity data, we used Burned Area Reflectance Classification image as a proxy indicator, as described in previous works [50,78,79]. To acquire BARC, we used dNBR raster data of the burned area as a basis following previous works [80–82]. In detail, BARC was derived by a resampling to unsigned 8-bit images of the raw dNBR dataset, generating a BARC256 layer with values between 0 and 255, using the following equation [83]:

$$\text{BARC256} = (\text{dNBR} + 275) / 5 \quad (6)$$

Then, BARC4 maps were generated by adjusting the BARC256 maps into a four categories, following previous publications [84], namely: unburned (BARC256 < 78), low (78 < BARC256 < 112), moderate (112 < BARC256 < 188), and high (BARC256 > 188), creating a 4-class thematic raster.

With regard to soil erodibility factor (K-factor), which in the U.S. application is derived by Schwartz and Alexander [85], we used a Europe-wide dataset published by Joint Research Centre of the European Commission and the European Soil Data Center (ES-DAC) [86] with a 500 m-resolution grid. We selected this dataset because of its spatial coverage, so that in our adaptation of the model, its application remains highly transferable to other locations in the region.

With regard to field observations, we visited the area at different times after storms in the post-fire period, namely: on 10 and 15 October, on 19, 24 and 26 November, as well as on 11 and 29 December in the autumn and winter of 2021 to record possible mass movement phenomena triggered by storms. In terms of rainfall accumulation these

October events recorded 11 mm and 21 mm, respectively, whereas the November ones recorded 24.0 mm, 16.0 mm and 34.2 mm, respectively. The aforementioned December storms recorded 19.4 mm and 23.0 mm, respectively. In the course of these field surveys, we in fact recorded sediment flows on 26 November in the form of debris flow generation at specific locations along the main channel of certain basins, reaching the respective outlets. Figure 4 illustrates debris flow phenomena recorded on 26 November 2021 near Vamvakies village (exact location details shown in the next section).

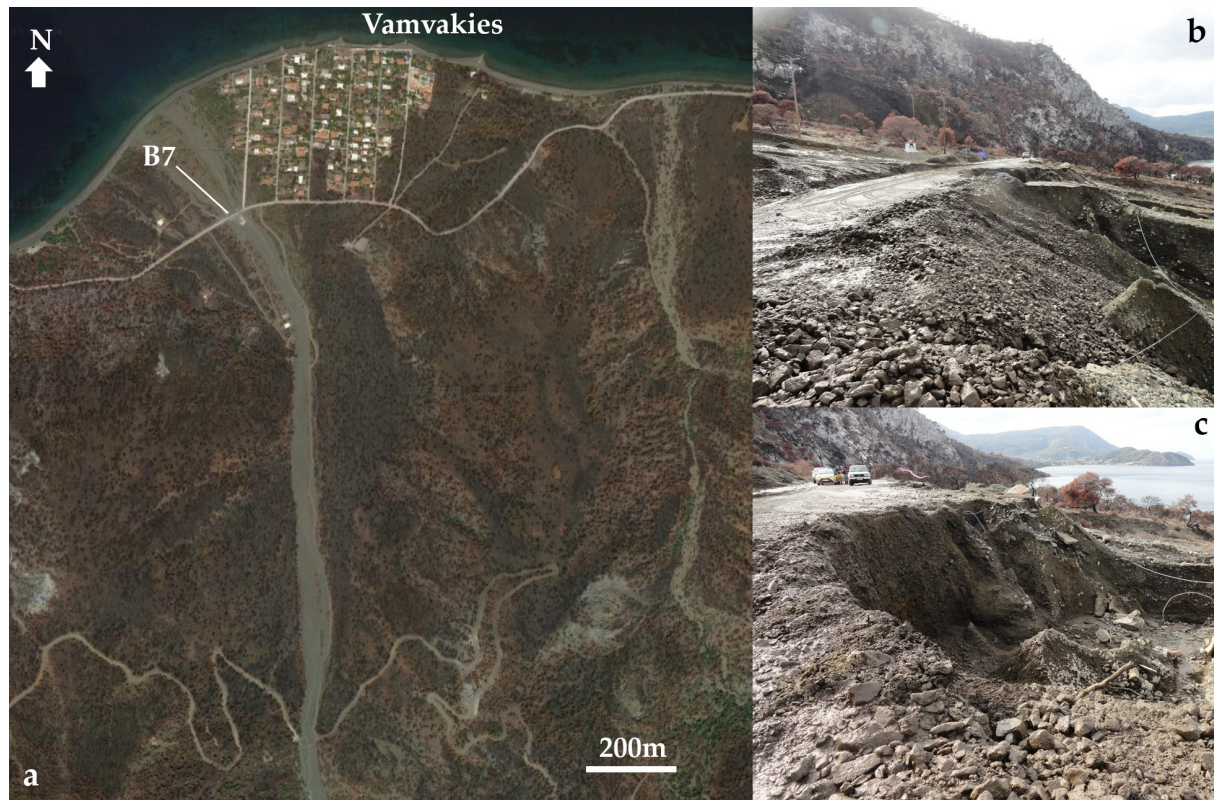


Figure 4. Characteristic image of a debris flow occurrence in the study area after the 26 November 2021 storm, (a) via satellite imagery [67] and (b,c) via ground observations at the outlet of basin B7.

With regard to validation, we used the ROC analysis [87,88] which has been used before in mass movement phenomena modeling and post-fire debris flow studies [40,89,90], as well as statistical tests, to explore a possible statistical difference between the likelihood calculated in each catchment and the actual debris flow generation findings from the field surveys.

In summary, the methodological steps of the present work include:

1. Collection of elevation and slope raster data, 15 min design rainfall data, and soil erodibility factor raster data of the study area;
2. Calculation of the dNBR index using satellite imagery of the burnt area and calculation of BARC4 soil burn severity raster data (based on the dNBR index);
3. Calculation of probability value for each basin by applying the Staley et al. [50] model (i.e., Equations (1)–(3));
4. Identification of debris flow generation through field survey;
5. Statistical tests and ROC analysis to explore a potential statistical association between the calculated probability and the actual debris flow occurrences identified in the field (step 4).

4. Results

Based on the above equations, we calculated the statistical likelihood of debris flow occurrence in 21 basins along the coastal road from Alepochori to Schinos, for a given maximum 15 min design rainfall accumulation. The probability (P) ranged from 0.05 to 0.893, with an average of 0.485.

Subsequently, five classes of equal interval were defined for the probability P obtained for cartographic illustration purposes, a practice followed also in previous works [70], namely: (1) 0–0.2: slightly probable, (2) 0.2–0.4: moderately probable, (3) 0.4–0.6: probable, (4) 0.6–0.8: very probable, (5) 0.8–1.0: highly probable. The following map (Figure 5) shows the probability in the study basins.

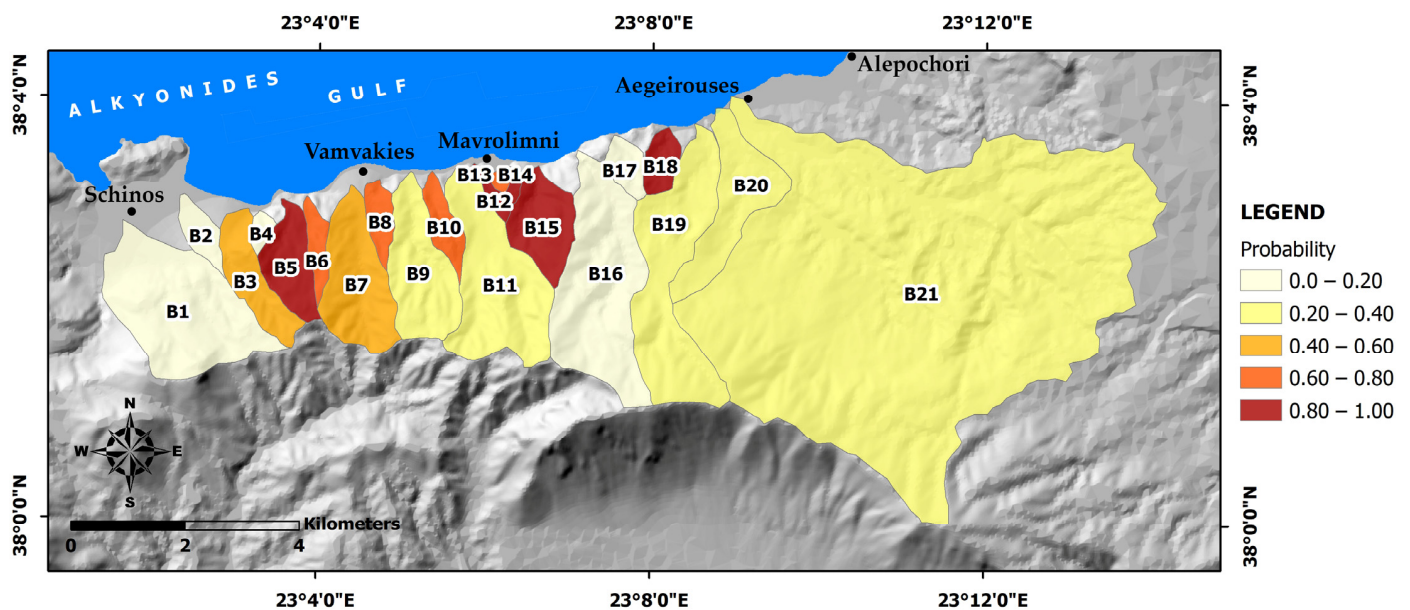


Figure 5. Map of the study area, with the values of the probability in each basin. The names B1 to B21 represent the codename of each basin.

Figure 6, shows characteristic images from the debris flows occurrences identified after the storm of 26 November 2021 at the outlet of basins B7, B12 and B13 near Vamvakies and Mavrolimni port (Figure 6a,b), between Schinos and Vamvakies villages at the outlets of basins B5 and B6 (Figure 6c,d,h) and at the outlets of basins B8, B14, and B15 (Figure 6e–g, respectively).

Comparison of debris flow occurrence with the probability of occurrence calculated based on the above equations shows initially correlation (Figures 7 and 8), as we identified debris flows at the outlet of eight basins (namely: B5, B14, B12, B15, B6, B13, B8, B7), based on field observations, all in basins with relatively high debris-flow occurrence probability.

To explore the statistical significance of this association, we examined the variable of probability against the actual catchment binary response (i.e., debris flow generation or no debris flow generation) through a Mann–Whitney U test. The test showed a statistically association between the two variables (sig. = 0.001), indicating a statistically significant difference between the value of probability in the basins, where we recorded a debris flow generation, and the basins that we did not.

In addition, we examined the predictive ability of the model, testing with the actual debris flow occurrences (true positives), through the Receiver Operating Characteristic (ROC) graph curves (Figure 9). The analysis revealed a fairly good model prediction accuracy with an AUC (area under the curve) value of 0.913. In this study, the ROC graph and the AUC value were derived using the ArcSDM tools in ArcGIS 10.7 software.



Figure 6. Debris flow occurrence in multiple locations across the study area, namely: (a) along the road from Vamvakies to Schinos, in the southwest edge of Vamvakies settlement (outlet of basin B7), (b) in Mavrolimni small port (near the outlets of basins B12 and B13), (c) along the road between Schinos and Vamvakies at the outlet of basin B6, (d,h) at the outlet of basin B5, and (e) at the outlet of basin B8, (f) along the road from Mavrolimni to Alepochori at the outlet of basin B14, and (g) at the outlet of basin B15.

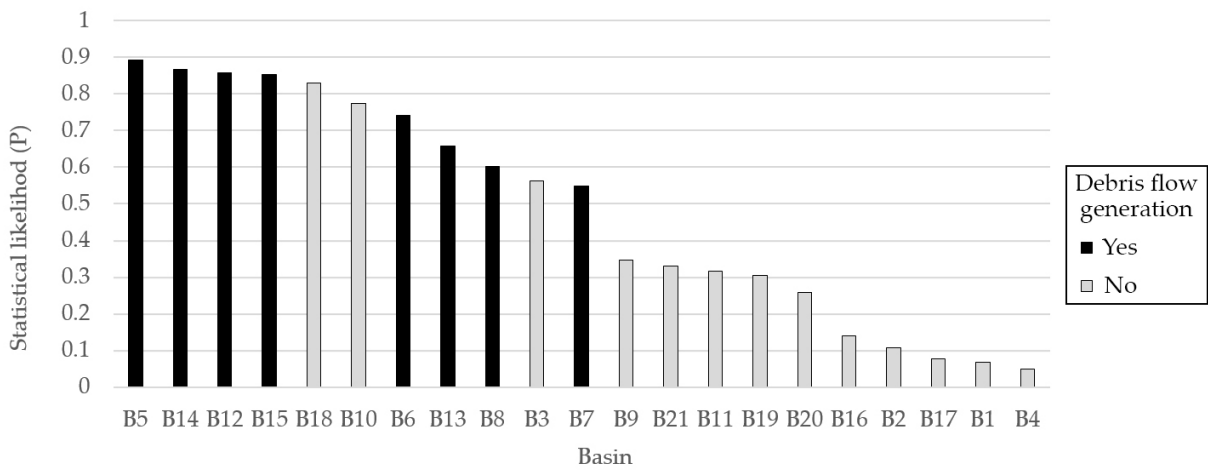


Figure 7. Graph of probabilities per basins, against debris flow occurrence.

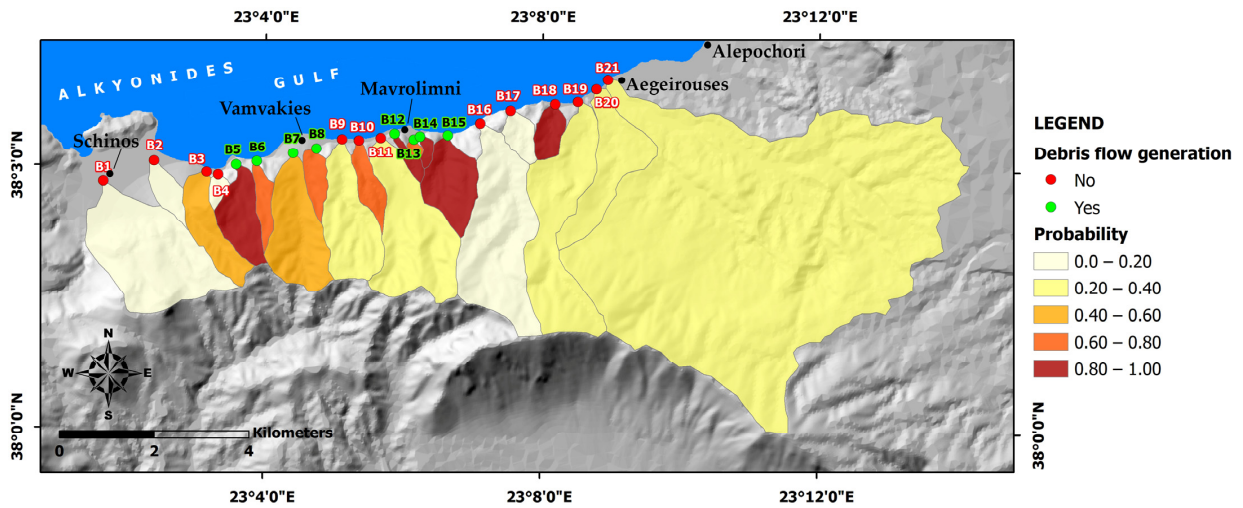


Figure 8. Map of the study area, showing the calculated probability of debris flow occurrence in five categories, against the actual debris flows (DB) generation during the 21 December storm in the area. The names B1 to B21 represent the codename of each basin.

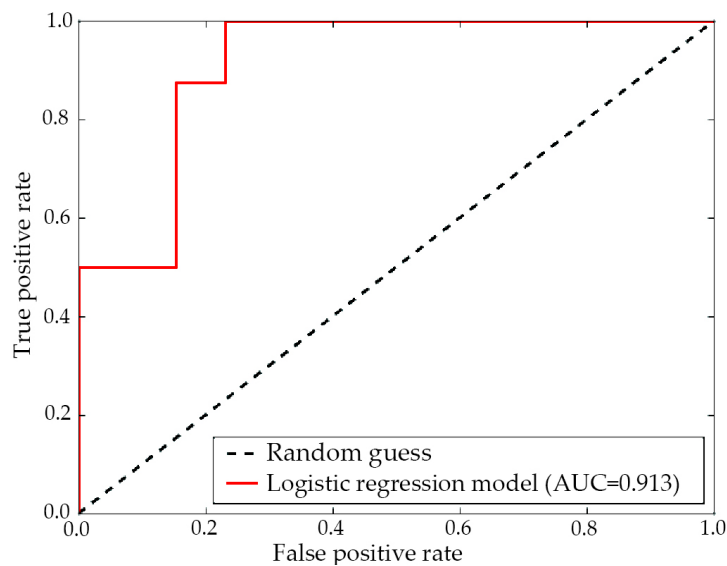


Figure 9. ROC graph showing the logistic regression model performance against the true positives of debris flow actual occurrence locations in the study area. AUC (Area Under the Curve) equals 0.913.

5. Discussion

This work explores the applicability of a logistic regression model for debris flow generation prediction in Greece, as a characteristic example of the Eastern Mediterranean region landscape, using the post-fire environment of Schinos fire-hit area as a case study. In this study, a model already in use in the western U.S. was selected (Staley et al. [50]), with an adaptation of involving a European dataset of soil erodibility data (K-factor). Overall, the findings show that the model is able to provide results in the terrain of the study area, as a characteristic example of the Eastern Mediterranean region, preliminarily indicating a good match with debris flow occurrence in the area (i.e., statistical association and other criteria used). The findings are a strong indication that the model in question can be further used in the area in a more systematic way to assess debris flow risk immediately after forest fires. The results indicate that the model can function with established European K-factor datasets [86], which is a critical point when it comes to retaining a high transferability of the approach.

The model tested has relatively low data requirements and therefore is more desirable for rapid assessment of the situation. This is particularly useful for authorities and the local communities, as they strive to find and use all the available tools and methods to deal effectively with fire-induced hazards that can potentially appear in the next rainfall season [91–93] (i.e., in a short period), as recorded in fire-hit areas in the past [5]. These characteristics are useful in the sense of allowing a rapid assessment of debris flow likelihood that provides the foundation for planning and especially prioritizing interventions (i.e., post-fire measures) given that their development is time-sensitive. Thus, this model fits the needs for a tool functioning within the context of limited time and data availability.

Furthermore, in terms of advantages and improved prediction of debris flow occurrence and intensity, allows for better preparation and mitigation of the potential damage they can cause. Enhanced ability to identify areas of high risk and design targeted protective measures at those particular locations to reduce the impact of debris flows.

In addition, given that such hazard can persist for several years after the actual fire, increased awareness of the effects of debris flows on the environment and the locations of high risk, allow for more effective management and conservation of resources, including better decision-making about land use and management as well as distribution and prioritization of funds. Moreover, a better understanding of debris flow risks, allows for informed decision making when it comes to infrastructure effective design and maintenance strategies, the foundation to a more robust infrastructure network, able to withstand such dangerous phenomena [94,95]. Further, improving the spatial understanding of risks has the potential to enable a more effective disaster response, allowing the emergency or civil protection authorities to focus on the more sensitive areas or the basins with higher debris flow generation probabilities. For example, by restricting access to dangerous parts of the road network prior to an expected high-intensity storm.

One of the advantages of the approach used is that it provides results in a geospatial form, creating maps that can be understood and communicated more easily to local stakeholders, authorities and even towards the public [96]. Moreover, the approach can function in terrains characterized by the small-sized catchments, with dense infrastructure and population, high resolution results are needed [97,98]. This fits the geo-environmental setting of the Eastern Mediterranean and of Greece in particular, with its mountainous terrain, dominated by high-inclination, ephemeral streams and complex alternating lithologies.

With regard to limitations, a primary source of uncertainty concerns the small sample of basins and debris flow occurrences analyzed in the present study. The present application bears an added value for exploring the applicability of the approach, especially given the field validation data. However, future research in the region would benefit from including a larger number of catchments aiming to collect more data with the potential to improve the empirically derived parameters of the model to fit better in the region, a process that took several years in the Western U.S. applications. One additional limitation in the current application of the model is the selection and use of a single value for the 15 min rainfall

accumulation. Given the small differences in values and distance of the neighboring stations as well as the small size of the study area, it is expected to have a negligible effect in the overall calculation of the statistical likelihood across the different catchments examined. However, it has to be noted that applications in larger study areas should include the spatial variability of the design rainfall. Moreover, it is important to note that small high-intensity increments in rainfall (e.g., 5 min peaks) may be associated with debris flow generation locally [99], indicating that beyond 15 min rainfall accumulation values, rainfall data of higher temporal resolution could be interesting to explore as well. In addition, it has to be mentioned that the use of pan-European soil data, in the present study, bears limitations that are associated with the methodological assumptions of this dataset development and its resolution [86]. Specifically, it has to be noted that local high-resolution soil datasets can be used instead of the relatively coarser resolution European-wide ones, used in the present study to describe the soil erodibility. However, considering the European dataset's extent and its wide usage, as well as the relatively low spatial variability of values of soil erodibility (in comparison for example with elevation or slope) this tradeoff is considered beneficial for the transferability and the standardization of the approach.

6. Conclusions

This work explores the applicability of a binary regression model for debris flow generation statistical likelihood assessment in Greece, as a characteristic example of the Eastern Mediterranean terrain. The results together with the field validation, by means of field observations of actual debris flow occurrence in the study area, show that the method can function within the particular geo-environmental characteristics of the study area, indicating that this approach can be used in more extensive applications in the region, in terms of area covered. The calculated probability ranged from 0.05 to 0.893, with an average of 0.485, with 11 out of 21 basins presenting relatively higher values. Eight out of these eleven basins experienced a debris flow in the period studied, showing a statistically significant association ($\text{sig} = 0.001$) and a high AUC value (0.913) in a ROC analysis. The model is considered highly transferable, taking into consideration that it has relatively limited data requirements, uses easily available geospatial data and can function well with the adaptation of using established European soil datasets (K-factor). These features support its applicability across the region. Moreover, the application of the model fits the context of rapid assessment that is required immediately after a fire, helping to take informed decisions regarding implementing measures or other risk management initiatives in the short time available between summer fire season and autumn–winter rainfall period that follows.

The application of such models has the potential to lead to improved hazard assessment and through it, better and more effective risk management. A better prediction of debris flows is critical in the Mediterranean region and has the potential to enable a more informed resource management, prioritization and planning of interventions, effective design of infrastructure and prevention of high-risk situations especially involving human lives. The systematic use of such a tool can contribute to the overall efforts to reduce exposure of people, infrastructure, and important natural, cultural, and economic resources to these hazards.

Supplementary Materials: The following supporting information can be downloaded at: <https://www.mdpi.com/article/10.3390/land12030555/s1>, Figure S1: title Geological map of the study area, illustrating alpine and post-alpine formations and the active faults; Figure S2: Characteristic viewpoints of the burnt area near the coast, showing (a,b) high inclination slopes typical of the study area, (c,d) views from uphill with slopes covered by loose material – rocks and soil, (e) the main road axis crossing the burnt area, and (f) the boundary of the fire along the burnt slope neighboring the beach. At the hill at the far end of the picture is Schinos village (f).

Author Contributions: Conceptualization, M.D. and S.M.; methodology, M.D., S.M., E.V. and V.C.; software, E.V.; validation, M.D., S.M., E.V. and V.C.; formal analysis, M.D. and S.M.; investigation, M.D., S.M., E.V. and V.C.; resources, M.D.; data curation, E.V. and V.C.; writing—original draft preparation, M.D., S.M. and E.V.; writing—review and editing, M.D. and S.M.; visualization, M.D., S.M. and E.V. All authors have read and agreed to the published version of the manuscript.

Funding: This research received no external funding.

Data Availability Statement: Data available upon request.

Conflicts of Interest: The authors declare no conflict of interest.

References

1. Shakesby, R.A. Post-wildfire soil erosion in the Mediterranean: Review and future research directions. *Earth-Sci. Rev.* **2011**, *105*, 71–100. [\[CrossRef\]](#)
2. Moody, J.A.; Shakesby, R.A.; Robichaud, P.R.; Cannon, S.H.; Martin, D.A. Current research issues related to post-wildfire runoff and erosion processes. *Earth-Sci. Rev.* **2013**, *122*, 10–37. [\[CrossRef\]](#)
3. Neary, D.G. Wildfire contribution to desertification at local, regional, and global scales. *Desertif. Past Curr. Future Trends* **2018**, *10*, 199–222.
4. Neary, D.G. Post-wildland fire desertification: Can rehabilitation treatments make a difference? *Fire Ecol.* **2009**, *5*, 129–144. [\[CrossRef\]](#)
5. Diakakis, M.; Nikolopoulos, E.I.; Mavroulis, S.; Vassilakis, E.; Korakaki, E. Observational evidence on the effects of mega-fires on the frequency of hydrogeomorphic hazards. The case of the Peloponnese fires of 2007 in Greece. *Sci. Total Environ.* **2017**, *592*, 262–276. [\[CrossRef\]](#)
6. Jong-Levinger, A.; Banerjee, T.; Houston, D.; Sanders, B.F. Compound Post-Fire Flood Hazards Considering Infrastructure Sedimentation. *Earth's Future* **2022**, *10*, 848–866. [\[CrossRef\]](#)
7. De Graff, J.V. Improvement in quantifying debris flow risk for post-wildfire emergency response. *Geoenviron. Disasters* **2014**, *1*, 1–10. [\[CrossRef\]](#)
8. Parise, M.; Cannon, S.H. Wildfire impacts on the processes that generate debris flows in burned watersheds. *Nat. Hazards* **2012**, *61*, 217–227. [\[CrossRef\]](#)
9. Nyman, P.; Smith, H.G.; Sherwin, C.B.; Langhans, C.; Lane, P.N.J.; Sheridan, G.J. Predicting sediment delivery from debris flows after wildfire. *Geomorphology* **2015**, *250*, 173–186. [\[CrossRef\]](#)
10. Cannon, S.H.; Gartner, J.E. Wildfire-related debris flow from a hazards perspective. In *Debris-Flow Hazards and Related Phenomena*; Springer: Berlin/Heidelberg, Germany, 2005; pp. 363–385.
11. Zhao, L.; He, J.W.; Yu, Z.X.; Liu, Y.P.; Zhou, Z.H.; Chan, S.L. Coupled numerical simulation of a flexible barrier impacted by debris flow with boulders in front. *Landslides* **2020**, *17*, 2723–2736. [\[CrossRef\]](#)
12. Jakob, M.; Stein, D.; Ulmi, M. Vulnerability of buildings to debris flow impact. *Nat. Hazards* **2012**, *60*, 241–261. [\[CrossRef\]](#)
13. Scheidl, C.; Chiari, M.; Kaitna, R.; Müllegger, M.; Krawtschuk, A.; Zimmermann, T.; Proske, D. Analysing Debris-Flow Impact Models, Based on a Small Scale Modelling Approach. *Surv. Geophys.* **2013**, *34*, 121–140. [\[CrossRef\]](#)
14. Santi, P.M.; Hewitt, K.; VanDine, D.F.; Cruz, E.B. Debris-flow impact, vulnerability, and response. *Nat. Hazards* **2011**, *56*, 371–402. [\[CrossRef\]](#)
15. Nam, D.H.; Kim, M.-I.; Kang, D.H.; Kim, B.S. Debris flow damage assessment by considering debris flow direction and direction angle of structure in South Korea. *Water* **2019**, *11*, 328. [\[CrossRef\]](#)
16. Lancaster, J.T.; Swanson, B.J.; Lukashov, S.G.; Oakley, N.S.; Lee, J.B.; Spangler, E.R.; Hernandez, J.L.; Olson, B.P.E.; DeFrisco, M.J.; Lindsay, D.N.; et al. Observations and Analyses of the 9 January 2018 Debris-Flow Disaster, Santa Barbara County, California. *Environ. Eng. Geosci.* **2021**, *27*, 3–27. [\[CrossRef\]](#)
17. Shakesby, R.A.; Doerr, S.H. Wildfire as a hydrological and geomorphological agent. *Earth-Sci. Rev.* **2006**, *74*, 269–307. [\[CrossRef\]](#)
18. Dorn, R.I. Boulder weathering and erosion associated with a wildfire, Sierra Ancha Mountains, Arizona. *Geomorphology* **2003**, *55*, 155–171. [\[CrossRef\]](#)
19. Ice, G.G.; Neary, D.G.; Adams, P.W. Effects of Wildfire on Processes. *J. For.* **2004**, *102*, 16–20.
20. Cardenas, M.B.; Kanarek, M.R. Soil moisture variation and dynamics across a wildfire burn boundary in a loblolly pine (*Pinus taeda*) forest. *J. Hydrol.* **2014**, *519*, 490–502. [\[CrossRef\]](#)
21. Doerr, S.H.; Shakesby, R.A.; Walsh, R.P.D. Soil water repellency: Its causes, characteristics and hydro-geomorphological significance. *Earth Sci. Rev.* **2000**, *51*, 33–65. [\[CrossRef\]](#)
22. Woods, S.W.; Balfour, V.N. The effect of ash on runoff and erosion after a severe forest wildfire, Montana, USA. *Int. J. Wildl. Fire* **2008**, *17*, 535–548. [\[CrossRef\]](#)
23. Larsen, I.J.; Pederson, J.L.; Schmidt, J.C. Geologic versus wildfire controls on hillslope processes and debris flow initiation in the Green River canyons of Dinosaur National Monument. *Geomorphology* **2006**, *81*, 114–127. [\[CrossRef\]](#)
24. Tiranti, D.; Cremonini, R.; Sanmartino, D. Wildfires effect on debris flow occurrence in italian western alps: Preliminary considerations to refine debris flow early warnings system criteria. *Geosciences* **2021**, *11*, 422. [\[CrossRef\]](#)

25. Pellegrino, A.M.; Schippa, L. Rheological modeling of macro viscous flows of granular suspension of regular and irregular particles. *Water* **2017**, *10*, 21. [[CrossRef](#)]
26. Alfieri, L.; Salamon, P.; Pappenberger, F.; Wetterhall, F.; Thielen, J. Operational early warning systems for water-related hazards in Europe. *Environ. Sci. Policy* **2012**, *21*, 35–49. [[CrossRef](#)]
27. Tiranti, D.; Rabuffetti, D. Estimation of rainfall thresholds triggering shallow landslides for an operational warning system implementation. *Landslides* **2010**, *7*, 471–481. [[CrossRef](#)]
28. Guzzetti, F.; Peruccacci, S.; Rossi, M.; Stark, C.P. The rainfall intensity-duration control of shallow landslides and debris flows: An update. *Landslides* **2008**, *5*, 3–17. [[CrossRef](#)]
29. Bezak, N.; Mikoš, M. Changes in the rainfall event characteristics above the empirical global rainfall thresholds for landslide initiation at the pan-European level. *Landslides* **2021**, *18*, 1859–1873. [[CrossRef](#)]
30. Molina-Terrén, D.M.; Xanthopoulos, G.; Diakakis, M.; Ribeiro, L.; Caballero, D.; Delogu, G.M.; Viegas, D.X.; Silva, C.A.; Cardil, A. Analysis of forest fire fatalities in Southern Europe: Spain, Portugal, Greece and Sardinia (Italy). *Int. J. Wildl. Fire* **2019**, *28*, 85–98. [[CrossRef](#)]
31. Eftimiou, N.; Psomiadis, E.; Panagos, P. Fire severity and soil erosion susceptibility mapping using multi-temporal Earth Observation data: The case of Mati fatal wildfire in Eastern Attica, Greece. *Catena* **2020**, *187*, 104320. [[CrossRef](#)]
32. Diakakis, M.; Xanthopoulos, G.; Gregos, L. Analysis of forest fire fatalities in Greece: 1977–2013. *Int. J. Wildl. Fire* **2016**, *25*, 797–809. [[CrossRef](#)]
33. Abatzoglou, J.T.; Kolden, C.A. Climate change in Western US deserts: Potential for increased wildfire and invasive annual grasses. *Rangel. Ecol. Manag.* **2011**, *64*, 471–478. [[CrossRef](#)]
34. Canuti, P.; Margottini, C.; Fanti, R.; Bromhead, E.N. *Cultural Heritage and Landslides: Research for Risk Prevention and Conservation*; Springer: Berlin/Heidelberg, Germany, 2009; ISBN 9783540699668.
35. Di Virgilio, G.; Evans, J.P.; Blake, S.A.P.; Armstrong, M.; Dowdy, A.J.; Sharples, J.; McRae, R. Climate Change Increases the Potential for Extreme Wildfires. *Geophys. Res. Lett.* **2019**, *46*, 8517–8526. [[CrossRef](#)]
36. Cannon, S.H.; DeGraff, J. The Increasing Wildfire and Post-Fire Debris-Flow Threat in Western USA, and Implications for Consequences of Climate Change. In *Landslides–Disaster Risk Reduction*; Sassa, K., Canuti, P., Eds.; Springer: Berlin/Heidelberg, Germany, 2009; pp. 177–190.
37. Hoch, O.J.; McGuire, L.A.; Youberg, A.M.; Rengers, F.K. Hydrogeomorphic Recovery and Temporal Changes in Rainfall Thresholds for Debris Flows Following Wildfire. *J. Geophys. Res. Earth Surf.* **2021**, *126*. [[CrossRef](#)]
38. Mayor, A.G.; Bautista, S.; Llovet, J.; Bellot, J. Post-fire hydrological and erosional responses of a Mediterranean landscape: Seven years of catchment-scale dynamics. *Catena* **2007**, *71*, 68–75. [[CrossRef](#)]
39. Cannon, S.H.; Gartner, J.E.; Wilson, R.C.; Bowers, J.C.; Laber, J.L. Storm rainfall conditions for floods and debris flows from recently burned areas in southwestern Colorado and southern California. *Geomorphology* **2008**, *96*, 250–269. [[CrossRef](#)]
40. Staley, D.M.; Kean, J.W.; Cannon, S.H.; Schmidt, K.M.; Laber, J.L. Objective definition of rainfall intensity-duration thresholds for the initiation of post-fire debris flows in southern California. *Landslides* **2013**, *10*, 547–562. [[CrossRef](#)]
41. Berti, M.; Bernard, M.; Gregoretti, C.; Simoni, A. Physical Interpretation of Rainfall Thresholds for Runoff-Generated Debris Flows. *J. Geophys. Res. Earth Surf.* **2020**, *125*, e2019JF005513. [[CrossRef](#)]
42. Marra, F.; Nikolopoulos, E.I.; Creutin, J.D.; Borga, M. Space–time organization of debris flows-triggering rainfall and its effect on the identification of the rainfall threshold relationship. *J. Hydrol.* **2016**, *541*, 246–255. [[CrossRef](#)]
43. Staley, D.M.; Negri, J.A.; Kean, J.W.; Laber, J.L.; Tillery, A.C.; Youberg, A.M. Prediction of spatially explicit rainfall intensity–duration thresholds for post-fire debris-flow generation in the western United States. *Geomorphology* **2017**, *278*, 149–162. [[CrossRef](#)]
44. D’Amato Avanzi, G.; Giannecchini, R.; Puccinelli, A. The influence of the geological and geomorphological settings on shallow landslides. An example in a temperate climate environment: The June 19, 1996 event in northwestern Tuscany (Italy). *Eng. Geol.* **2004**, *73*, 215–228. [[CrossRef](#)]
45. Zhang, Y.; Ge, T.; Tian, W.; Liou, Y.-A. Debris Flow Susceptibility Mapping Using Machine-Learning Techniques in Shigatse Area, China. *Remote Sens.* **2019**, *11*, 2801. [[CrossRef](#)]
46. Destro, E.; Amponsah, W.; Nikolopoulos, E.I.; Marchi, L.; Marra, F.; Zocatelli, D.; Borga, M. Coupled prediction of flash flood response and debris flow occurrence: Application on an alpine extreme flood event. *J. Hydrol.* **2018**, *558*, 225–237. [[CrossRef](#)]
47. Nikolopoulos, E.I.; Destro, E.; Bhuiyan, A.E.; Borga, M.; Anagnostou, E.N. Evaluation of predictive models for post-fire debris flow occurrence in the western United States. *Nat. Hazards Earth Syst. Sci.* **2018**, *18*, 2331–2343. [[CrossRef](#)]
48. Wall, S.; Murphy, B.P.; Belmont, P.; Yocom, L. Predicting post-fire debris flow grain sizes and depositional volumes in the Intermountain West, United States. *Earth Surf. Process. Landf.* **2023**, *48*, 179–197. [[CrossRef](#)]
49. Cannon, S.H.; Gartner, J.E.; Rupert, M.G.; Michael, J.A.; Rea, A.H.; Parrett, C. Predicting the probability and volume of postwildfire debris flows in the intermountain western United States. *Bull. Geol. Soc. Am.* **2010**, *122*, 127–144. [[CrossRef](#)]
50. Staley, D.M.; Negri, J.A.; Kean, J.W.; Laber, J.M.; Tillery, A.C.; Youberg, A.M. *Updated Logistic Regression Equations for the Calculation of Post-Fire Debris-Flow Likelihood in the Western United States, Open-File Report 2016-1106*; USGS: Denver, CO, USA, 2016; 13p. [[CrossRef](#)]
51. Rupert, M.G.; Cannon, S.H.; Gartner, J.E.; Michael, J.A.; Helsel, D.R. *Using Logistic Regression to Predict a Probability of Debris Flows in Areas Burned by Wildfires, Southern California, 2003–2006. Open-File Report 2008-1370*; USGS: Denver, CO, USA, 2008. [[CrossRef](#)]

52. Bornovas, I.; Spyridopoulos, A.; Gaitanakis, P. *Geological Map of Greece, Scale 1:50.000, Perachora Sheet*; Institute of Geological and Mineral Exploration: Athens, Greece, 1984.
53. Bornovas, I.; Eleftheriou, A.; Gaitanakis, P.; Rondoyanni, T.; Simaeakis, K. *Geological Map of Greece, Scale 1:50.000, Kaparellion Sheet*; Institute of Geological and Mineral Exploration: Athens, Greece, 1984.
54. Gaitanakis, P.; Mettos, A.; Fytikas, M. *Geological Map of Greece, Scale 1:50.000, Sofiko Sheet*; Institute of Geological and Mineral Exploration: Athens, Greece, 1985.
55. Jackson, J.A.; Houseman, G.G.; King, G.C.P.; Papadimitriou, P.; Soufleris, C.; Virieux, J. Seismicity, normal faulting, and the geomorphological development of the Gulf of Corinth (Greece) the Corinth earthquakes. *Earth Planet. Sci. Lett.* **1982**, *57*, 377–397. [[CrossRef](#)]
56. Sakellariou, D.; Lykousis, V.; Papanikolaou, D. Neotectonic Structure and Evolution of the Gulf of Alkyonides, Central Greece. *Bull. Geol. Soc. Greece* **1998**, *32*, 241–250.
57. Leeder, M.R.; Collier, R.E.L.; Aziz, L.H.A.; Trout, M.; Ferentinos, G.; Papatheodorou, G.; Lyberis, E. Tectono-sedimentary processes along an active marine/lacustrine half-graben margin: Alkyonides Gulf, E. Gulf of Corinth, Greece. *Basin Res.* **2002**, *14*, 25–41. [[CrossRef](#)]
58. Taymaz, T.; Eyidoğan, H.; Jackson, J. Source parameters of large earthquakes in the East Anatolian Fault Zone (Turkey). *Geophys. J. Int.* **1991**, *106*, 537–550. [[CrossRef](#)]
59. Antonaki, R.; Vlachos, I.; Staurakakis, G.; Taflamba, I.; Tokas, I.; Chatziandreu, S.; Smpokos, I.; Karydis, P.; Kaleuras, B. *Earthquake economic impact – Insurance*; Report of Earthquake Planning and Protection Organization: Athens, Greece, 1988.
60. Mariolakos, I.; Papanikolaou, D. The neogene basins of the Aegean Arc from the paleogeographic and the geodynamic point of view. In *Proceedings of the International Symposium Hellenic Arc and Trench (HEAT)*, Athens, Greece, 8–10 April 1981; Volume 1, pp. 383–399.
61. Pirazzoli, P.A.; Stiros, S.C.; Arnold, M.; Laborel, J.; Laborel-Deguen, F.; Papageorgiou, S. Episodic uplift deduced from Holocene shorelines in the Perachora Peninsula, Corinth area, Greece. *Tectonophysics* **1994**, *229*, 201–209.
62. Dafis, S. *Classification of Forest Vegetation in Greece*; Agricultural and Forestry School, Aristotle University of Thessaloniki: Thessaloniki, Greece, 1973.
63. Kalliris, P.A. *Final Study of Erosion and Flood Control Measures for Burnt Forest Areas in the Area of Schinos Settlement of Schinou of the Pissia Community of the Loutraki-Perachora-Agioi Theodoroi Municipality of the Corinthia Regional Unit from the 19 May 2021 Fire*; Korinthos Forest Service: Corinth, Greece, 2021.
64. Lekkas, E.; Andreadakis, E.; Diakakis, M.; Spyrou, N.-I.; Kranis, H.; Vassilakis, E.; Katsetsiadou, K.-N.; Carydis, P.; Kosmopoulos, E.; Stamati, E.; et al. *The May 19, 2021, Schinos, Greece, Forest Fire*; University of Athens: Athens, Greece, 2021.
65. PANACEA PANhellenic Infrastructure for Atmospheric Composition and Climate Change (PANACEA). Available online: <https://air-quality.gr/> (accessed on 20 May 2021).
66. Copernicus Emergency Management. Copernicus Emergency Management Service EMSR510: Fire in Peloponnese and Attika Regions, Greece. Available online: <https://emergency.copernicus.eu/mapping/list-of-components/EMSR510> (accessed on 4 January 2023).
67. Planet. *Planet PlanetScope Imagery 2021*; Planet: San Francisco, CA, USA, 2021.
68. Heckmann, T.; Gegg, K.; Gegg, A.; Becht, M. Sample size matters: Investigating the effect of sample size on a logistic regression susceptibility model for debris flows. *Nat. Hazards Earth Syst. Sci.* **2014**, *14*, 259–278. [[CrossRef](#)]
69. Achour, Y.; García, S.; Cavaleiro, V. GIS-based spatial prediction of debris flows using logistic regression and frequency ratio models for Zêzere River basin and its surrounding area, Northwest Covilhã, Portugal. *Arab. J. Geosci.* **2018**, *11*, 550. [[CrossRef](#)]
70. U.S. Geological Survey Emergency Assessment of Post-Fire Debris-Flow Hazards: U.S. Geological Survey Landslide Hazards Program Web Page. Available online: http://landslides.usgs.gov/hazards/postfire_debrisflow/ (accessed on 4 January 2023).
71. Shmida, A. Mediterranean vegetation in California and Israel: Similarities and differences. *Isr. J. Bot.* **1981**, *30*, 105–123. [[CrossRef](#)]
72. Polade, S.D.; Gershunov, A.; Cayan, D.R.; Dettinger, M.D.; Pierce, D.W. Precipitation in a warming world: Assessing projected hydro-climate changes in California and other Mediterranean climate regions. *Sci. Rep.* **2017**, *7*, 1–10. [[CrossRef](#)]
73. Verhey, W.; Rosa, D. De Mediterranean Soils. In *Land Use, Land Cover and Soil Sciences*; Verhey, W., Ed.; UNESCO: Paris, France, 2006; Volume VII, pp. 1–10.
74. Goudie, A.S. *Arid and Semi-Arid Geomorphology*; Cambridge University Press: Cambridge, UK; New York, NY, USA, 2013.
75. Hellenic Cadastre. *Digital Elevation Model-DEM of the Large Scale Orthophotos Project*. *Open Data Portal*; Hellenic Cadastre: Athens, Greece, 2021.
76. Environmental Systems Research Institute. *ESRI ArcGIS Desktop—Release 10.7 2017*; Environmental Systems Research Institute: Redlands, CA, USA, 2017.
77. Special Secretariat for Water. *Flood Risk Management Plan. Stage I. 1st Phase—Deliverable No2. Intensity Duration Frequency Curves*; Ministry of Environment and Energy: Athens, Greece, 2018.
78. Lutes, D.C.; Keane, R.E.; Caratti, J.F.; Key, C.H.; Benson, N.C.; Sutherland, S.; Gangi, L.J. *Fire Effects Monitoring and Inventory System. Gen. Tech. Rep. RMRS-GTR-164-CD*; USDA: Fort Collins, CO, USA, 2006.
79. Ebel, B.A.; Romero, O.C.; Martin, D.A. Thresholds and relations for soil-hydraulic and soil-physical properties as a function of burn severity 4 years after the 2011 Las Conchas Fire, New Mexico, USA. *Hydrol. Process.* **2018**, *32*, 2263–2278. [[CrossRef](#)]

80. Key, C.H.; Bensons, N.C. *Landscape Assessment (LA) Sampling and Analysis Methods*; USDA Forest Service: Washington, DC, USA, 2006.
81. Keeley, J.E. Fire intensity, fire severity and burn severity: A brief review and suggested usage. *Int. J. Wildl. Fire* **2009**, *18*, 116–126. [[CrossRef](#)]
82. Robichaud, P.R.; Lewis, S.A.; Laes, D.Y.M.; Hudak, A.T.; Kokaly, R.F.; Zamudio, J.A. Postfire soil burn severity mapping with hyperspectral image unmixing. *Remote Sens. Environ.* **2007**, *108*, 467–480. [[CrossRef](#)]
83. Banister, K.; Chan, D.; Driscoll, J.M.; Fullerton, C.; Lien, A.; Lacroix, K.M. *Atlas of the Upper Gila River Watershed*; University of Arizona: Tucson, AZ, USA, 2014.
84. Romero, O.C.; Ebel, B.A.; Martin, D.A.; Buchan, K.W.; Jornigan, A.D. Postwildfire measurement of soil physical and hydraulic properties at selected sampling sites in the 2011 Las Conchas wildfire burn scar, Jemez Mountains, north-central New Mexico. *Sci. Investig. Rep.* **2018**, *48*. [[CrossRef](#)]
85. Schwartz, G.E.; Alexander, R.B. *State Soil Geographic (STATSGO) Data Base for the Conterminous United States Open-File Report 95-449*; USGS: Denver, CO, USA, 1995.
86. Panagos, P.; Meusburger, K.; Ballabio, C.; Borrelli, P.; Alewell, C. Soil erodibility in Europe: A high-resolution dataset based on LUCAS. *Sci. Total Environ.* **2014**, *479–480*, 189–200. [[CrossRef](#)]
87. Fawcett, T. An introduction to ROC analysis. *Pattern Recognit. Lett.* **2006**, *27*, 861–874. [[CrossRef](#)]
88. Swets, J.A. Measuring the Accuracy of Diagnostic Systems. *Science* **1988**, *240*, 1285–1293. [[CrossRef](#)]
89. Youberg, A.M. Modern and Ancient Debris Flows in Arizona. Ph.D. Thesis, University of Arizona, Tucson, AZ, USA, 2014; p. 236.
90. Mavroulis, S.; Diakakis, M.; Kranis, H.; Vassilakis, E.; Kapetanidis, V.; Spingos, I.; Kaviris, G.; Skourtsos, E.; Voulgaris, N.; Lekkas, E. Inventory of Historical and Recent Earthquake-Triggered Landslides and Assessment of Related Susceptibility by GIS-Based Analytic Hierarchy Process: The Case of Cephalonia (Ionian Islands, Western Greece). *Appl. Sci.* **2022**, *12*, 2895. [[CrossRef](#)]
91. Moreira, F.; Arianoutsou, M.; Vallejo, V.R.; de las Heras, J.; Corona, P.; Xanthopoulos, G.; Fernandes, P.; Papageorgiou, K. Setting the Scene for Post-Fire Management. In *Post-Fire Management and Restoration of Southern European Forests*; Moreira, F., Arianoutsou, M., Corona, P., de las Heras, J., Eds.; Springer: Dordrecht, The Netherlands; Berlin/Heidelberg, Germany; London, UK; New York, NY, USA, 2012; pp. 1–20, ISBN 9789400722071.
92. Jordan, P. Post-wildfire debris flows in southern British Columbia, Canada. *Int. J. Wildl. Fire* **2016**, *25*, 322–336. [[CrossRef](#)]
93. Mavsar, R.; Varela, E.; Corona, P.; Barbat, A.; Marsh, G. Economic, Legal and Social Aspects of Post-Fire Management. In *Post-Fire Management and Restoration of Southern European Forests*; Moreira, F., Arianoutsou, M., Corona, P., de las Heras, J., Eds.; Springer: Dordrecht, The Netherlands; Heidelberg, Germany; London, UK; New York, NY, USA, 2012; pp. 45–78.
94. Li, C.; Ding, L.; Fang, Q.; Chen, K.; Castro-Lacouture, D. Risk-informed knowledge-based design for road infrastructure in an extreme environment. *Knowl.-Based Syst.* **2021**, *216*, 106741. [[CrossRef](#)]
95. Ellingwood, B.R. Risk-informed condition assessment of civil infrastructure: State of practice and research issues. *Struct. Infrastruct. Eng.* **2005**, *1*, 7–18. [[CrossRef](#)]
96. Dransch, D.; Rotzoll, H.; Poser, K. The contribution of maps to the challenges of risk communication to the public. *Int. J. Digit. Earth* **2010**, *3*, 292–311. [[CrossRef](#)]
97. Tillery, A.C.; Darr, M.J.; Cannon, S.H.; Michael, J.A. *Estimated Probability of Postwildfire Debris Flows in the 2012 Whitewater–Baldy Fire Burn Area, Southwestern New Mexico*; US Department of the Interior, US Geological Survey: Reston, VA, USA, 2012.
98. Verdin, K.L.; Dupree, J.A.; Elliot, J.G. *Probability and Volume of Potential Postwildfire Debris Flows in the 2012 Waldo Canyon Burn Area near Colorado Springs, Colorado*; US Geological Survey: Reston, VA, USA, 2012.
99. Kean, J.W.; Staley, D.M.; Cannon, S.H. In situ measurements of post-fire debris flows in southern California: Comparisons of the timing and magnitude of 24 debris-flow events with rainfall and soil moisture conditions. *J. Geophys. Res. Earth Surf.* **2011**, *116*, 1–21. [[CrossRef](#)]

Disclaimer/Publisher’s Note: The statements, opinions and data contained in all publications are solely those of the individual author(s) and contributor(s) and not of MDPI and/or the editor(s). MDPI and/or the editor(s) disclaim responsibility for any injury to people or property resulting from any ideas, methods, instructions or products referred to in the content.